Establishing the kinetics of ballistic-to-diffusive transition using directional statistics

Pai Liu, William R. Heinson, Benjamin J. Sumlin, Kuan-Yu Shen, and Rajan K. Chakrabarty

Phys. Rev. E **97**, 042102 — Published 4 April 2018

DOI: 10.1103/PhysRevE.97.042102

Establishing the Kinetics of Ballistic-to-Diffusive Transition Using Directional Statistics

Pai Liu[1], *William R. Heinson*[1], *Benjamin J. Sumlin*[1], *Kuan-Yu Shen*[1] *and Rajan K. Chakrabarty*[1,2,*]

[1] Center for Aerosol Science and Engineering

Department of Energy, Environmental and Chemical Engineering

Washington University in St. Louis, Missouri, USA – 63130

[2] McDonnell Center for the Space Sciences

Washington University in St. Louis, Missouri, USA – 63130

* Address correspondence to Rajan K. Chakrabarty (E-mail: chakrabarty@wustl.edu)

ABSTRACT

We establish the kinetics of the ballistic-to-diffusive (BD) transition observed in 2-dimensional random walk using directional statistics. Directional correlation is parameterized using the walker's turning angle distribution which follows the commonly adopted wrapped Cauchy distribution (WCD) function. During the BD transition, the concentration factor (ρ) governing the WCD shape is observed to decrease from its initial value. We next analytically derive the relationship between effective ρ and time, which essentially quantifies the BD transition rate. The prediction of our kinetic expression agrees well with the empirical datasets obtained from correlated random walk simulation. We further connect our formulation with the conventionally used scaling relationship between the walker's mean-square displacement and time.

I. INTRODUCTION

A century ago, Einstein theorized the existence of a ballistic regime in Brownian motion at infinitesimally small timescales [1,2]. This prediction was recently validated in experiments involving high temporal-resolution particle-tracking techniques [2,3] or conducted in rarefied surrounding environment [4,5]. The ballistic-to-diffusive (BD) transition, however, is not limited to Brownian systems driven by thermal fluctuation. A vast body of multidisciplinary research findings have witnessed a transient ballistic regime before the full-development of diffusive motions. Examples include the random walk of atom clusters [6,7], particle advection in weak turbulence [8,9], bacterial migration [10] and animal foraging activities [11,12]. The kinetics of BD transition determines the critical timescale corresponding to the onset of diffusion and subsequent applicability of the diffusive approximation. Despite its wide practical significance, a generalized mathematical formulation of the transition kinetics remains elusive. Langevin's formulation, involving an exponentially decaying velocity auto-correlation function [1-3], has limited applicability in describing the BD transition observed in semi-empirical, non-Brownian systems. When formulating a generalized kinetic expression, the difficulty arises from the multitude of system-specific driving mechanisms, as well as the order-of-magnitude variances in system length-scales [7,8,10,11]. One viable approach is to interpret the BD transition from a statistical perspective, and past attempts have been made on this front using the central limit theorem (CLT) [7,13]. Although it can satisfactorily explain the diffusive tendency of the random walk at large timescale, CLT ultimately fails to capture and parameterize the transition kinetics.

Here we interpret the BD transition in 2-dimensional (2-d) space using directional statistics [14-16]. More specifically, the subject of investigation is the probability distribution (P) of the walker's turning angle (θ) which describes the correlation between the successive steps of motion. Experimentally, the acquisition of P(θ) is done using single-particle tracking techniques; currently, such techniques find extensive use in the study of cell dynamics [17-21]. In the field of ecology, knowledge of P(θ) is critical for in reconstructing the trajectory of animal movement based on which search strategies are inferred [11, 12]. Given the importance of P(θ), here, we emphasize its role on broadly characterizing stochastic motion itself. If the motion is strictly ballistic, angle θ could only take value of 0 and the probability density of θ = 0 is infinitely large; thus, P(θ) is a Dirac delta function written as δ(0) [11,14-16]. The 2-d diffusion, on the other hand, is random walk manifesting an equiprobability of θ within the complete range between $-\pi$ to π, and therefore, P(θ) is a constant function of 1/(2π) [11,14-16]. During the BD transition, the dissipation in the correlation of the random walk could be captured by the evolution of P(θ) from δ(0) to 1/(2π) when the timescale increases by order-of-magnitude. In directional statistics, one of the mathematical expressions that could capture this evolution is the wrapped Cauchy distribution (WCD) function [11,14-16]. Eq. (1) shows the formulation of WCD function centered at θ = 0,

$$P(\theta, \rho) = \frac{1-\rho^2}{2\pi[1+\rho^2-2\rho\cos(\theta)]};\ \theta \in (-\pi, \pi] \tag{1}$$

where $\rho \in [0, 1]$ is the concentration factor that governs the shape of the distribution [11,14-16]. When ρ approaches 1 and 0, the WCD function asymptotes to the two extremities, δ(0) and 1/(2π), respectively. The kinetics of BD transition could therefore be established by relating ρ with a timescale parameter.

We show in the subsequent paragraphs the BD transition observed in the stochastic motion which was numerically simulated using the correlated random walk (CRW) model. The transition is tracked using the time-evolution of the random walker's reorientation statistics, as well as the inflection observed in the scaling relationship of the walker's mean-square displacement. Next, we formulate the kinetics of BD transition by establishing the mathematical relationship between the effective value of ρ and timescale. We conclude this paper by connecting our kinetic formulation with the spatio-temporal scaling relationship conventionally adopted in previous work [1,2,6-12].

II. METHODS

The CRW simulation follows the procedure introduced in Refs [11,22]. A 2-dimensional (2-d) unbounded, Cartesian space was created and the random walker was initially placed at the origin O (x = 0, y = 0, t = 0), where x and y represent the 2-d coordinates. The parameter t represents simulation time which increments by unit timescale τ_1. At the beginning of each timestep, a turning angle θ is randomly generated per the WCD function governed by a fixed shape factor ρ_1, where subscript 1 indicates its correspondence to the unit timescale τ_1. The random generation of θ follows the cumulative inversion method outlined in Ref [22]. Next, the random walker moves according to the direction designated by θ with a constant step-length δ_1. The algorithm repeats this procedure until the last timestep $t_n = 10^6\tau_1$ is reached and the trajectory of the random walker is recorded as the set [$x(t)$, $y(t)$].

From the trajectory dataset [$x(t)$, $y(t)$], the walker's time-averaged mean-square displacement $\langle\delta^2\rangle$ was calculated in a manner similar to that introduced in Ref [23,24]:

$$\langle\delta^2\rangle = \frac{\tau_1}{t_n - \tau}\sum_{t=\tau_1}^{t_n-\tau}\left[\big(x(t+\tau) - x(t)\big)^2 + \big(y(t+\tau) - y(t)\big)^2\right] \tag{2}$$

where τ represents a finite time interval divisible by τ_1. The walker's turning angle θ corresponding to timescale τ was calculated from its trajectory, specifically every three successive locations written as $[x(t), y(t)]$, $[x(t+\tau), y(t+\tau)]$ and $[x(t+2\tau), y(t+2\tau)]$. The detailed numerical method for this calculation is included in appendix A. We next divided the complete range of θ from -π to π equally into 500 bins and obtained P(θ) empirically by counting the frequency of θ within each bin. The effective value of ρ at τ was determined by performing the least square fit to the corresponding P(θ) datasets per Eq. (1).

III. RESULTS AND DISCUSSION

Figure 1 shows the random walk generated using a WCD function with $\rho_1 = 0.95$. The walker's trajectories observed under different timescales are colored in gray [$\tau = \tau_1$] and black [$\tau = 10^3\tau_1$]. When τ increases by order-of-magnitude, the correlation between successive steps of the motion becomes elusive and a Brownian-like random walk behavior manifests.

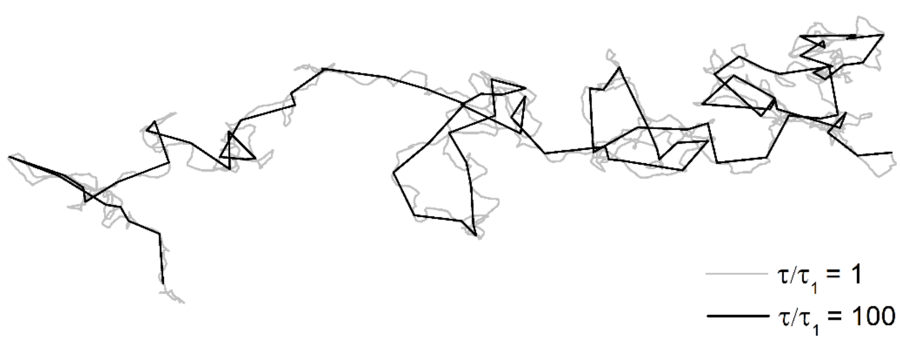

FIG 1. Examples of the random walk simulated using a WCD function with $\rho_1 = 0.95$. The walker's trajectories observed under normalized timescale $\tau/\tau_1 = 1$ and 10^3 are colored in gray and black, respectively.

Figure 2 (a) shows the scaling relationship between the walker's normalized mean-square displacement and timescale $\langle\delta^2\rangle/\delta_1^2 \propto (\tau/\tau_1)^\gamma$. The BD transition could be inferred from the inflection in the power-law relationship, which is signified by the decrease in the exponent γ from 2 to 1 [1,2,6-12]. Corresponding to the regime in which the inflection takes place, we show the evolution of the walker's P(θ) in Figure 2(b). When timescale of observation is small, for e.g. $\tau/\tau_1 = 4$, P(θ) is centralized at θ = 0 and manifests a sharp peak. With increase in τ/τ_1 by two orders of magnitude, P(θ) broadens and approaches uniformity. This evolution has been previously observed from particle tracking experiments conducted in biological systems [25]. Qualitatively, one could predict the onset of normal diffusion based on the increase in the width at half minimum of P(θ). Quantitatively, we performed least square fitting on the measured P(θ) datasets [circles] per the WCD function [red lines] and good agreement was observed. The effective value of ρ is seen to decrease from ρ_1 as τ/τ_1 increases [These values are labeled in the sub-panels of Figure 2 (b)].

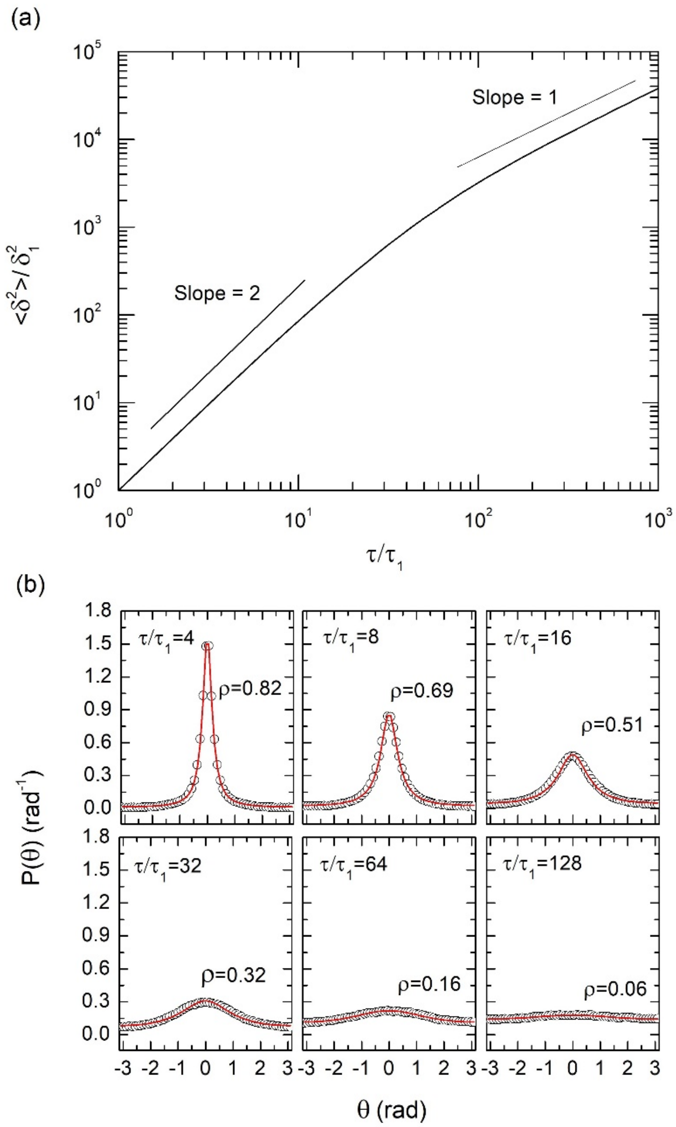

FIG. 2 (a) Normalized time-averaged mean-square displacement $\langle\delta^2\rangle/\delta_1^2$ as a function of normalized timescale τ/τ_1 for the random walk simulated with ρ_1 = 0.95. Straight lines in the log-log plot have slopes of 2 and 1, corresponding to the values of scaling exponent γ for ballistic motion and diffusion, respectively. (b) Evolution of the walker's turning angle distribution P(θ) with τ/τ_1 increasing from 4 to 128. Circles represent the P(θ) datasets empirically obtained from the CRW simulation. Red lines follow the WCD function [Eq. (1)] parameterized by the corresponding values of ρ shown in each subpanel.

The WCD function is not only limited to parameterizing the shape of P(θ) at unit timescale, it also accurately predicts the evolution of distribution shape with increasing τ. We analytically derive the mathematical relationship between the effective ρ value and τ. Our derivation is based on correlating the probability density of turning angles observed with increasing timescales as:

$$\tau_{2\mathrm{i}} = 2\tau_{\mathrm{i}} \tag{3}$$

where τ_{i} represents any arbitrary timescale and $\tau_{2\mathrm{i}}$ represents the timescale twice larger than τ_{i}. Our goal here is to establish the relationship between the corresponding $\rho_{2\mathrm{i}}$ and ρ_{i}. Figure 3(a) shows that when the motion is observed with timescale τ_{i}, the random walker is seen at five successive locations [black dots]. From these five locations, three successive turning angles could be identified and they are written as $\theta_{\mathrm{i},1}$, $\theta_{\mathrm{i},2}$ and $\theta_{\mathrm{i},3}$. When the timescale increases by two [that is $\tau_{2\mathrm{i}}$], the walker could only be seen at three locations [blue dots in Figure 3(b)], giving rise to one turning angle written as $\theta_{2\mathrm{i}}$. This geometric presentation in Figure 3 implies that once three successive turning angles $\{\theta_{\mathrm{i},1}, \theta_{\mathrm{i},2}, \theta_{\mathrm{i},3}\}$ are observed at any timescale, one definite turning angle $\theta_{2\mathrm{i}}$ will be conceived at the timescale twice larger. Assuming the magnitude of displacement δ_{i} during τ_{i} to be constant, those turning angles could be related per the following relationship:

$$\theta_{2\mathrm{i}} = \theta_{\mathrm{i},2} + \frac{1}{2}(\theta_{\mathrm{i},1} + \theta_{\mathrm{i},3}) \tag{4}$$

where counter clock-wise is regarded as the positive direction for angles. Noting the probabilities for the onset of $\theta_{\mathrm{i},1}$, $\theta_{\mathrm{i},2}$ and $\theta_{\mathrm{i},3}$ to be $P(\theta_{\mathrm{i},1})$, $P(\theta_{\mathrm{i},2})$ and $P(\theta_{\mathrm{i},3})$, respectively, we write the probability for the successive occurrence of $\{\theta_{\mathrm{i},1}, \theta_{\mathrm{i},2}, \theta_{\mathrm{i},3}\}$ as the product $P(\theta_{\mathrm{i},1})P(\theta_{\mathrm{i},2})P(\theta_{\mathrm{i},3})$. Here we assumed the onset of successive turning angles to be independent events, which differs fundamentally from the persistent random walk model introduced and adopted elsewhere [26]. The probability $P(\theta_{2\mathrm{i}})$ then could be calculated by summing $P(\theta_{\mathrm{i},1})P(\theta_{\mathrm{i},2})P(\theta_{\mathrm{i},3})$ for all exclusive combinations of $\{\theta_{\mathrm{i},1}, \theta_{\mathrm{i},2}, \theta_{\mathrm{i},3}\}$ that satisfies Eq. (4). This relationship could be written as:

$$P(\theta_{2i}, \rho_{2i}) = \sum_{\theta_{i,2}+\frac{1}{2}(\theta_{i,1}+\theta_{i,3})=\theta_{2i}} P(\theta_{i,1}, \rho_i)P(\theta_{i,2}, \rho_i)P(\theta_{i,3}, \rho_i) \tag{5}$$

Solving Eq. (5) with any arbitrary θ_{2i} yields the relationship between ρ_{2i} and ρ_i.

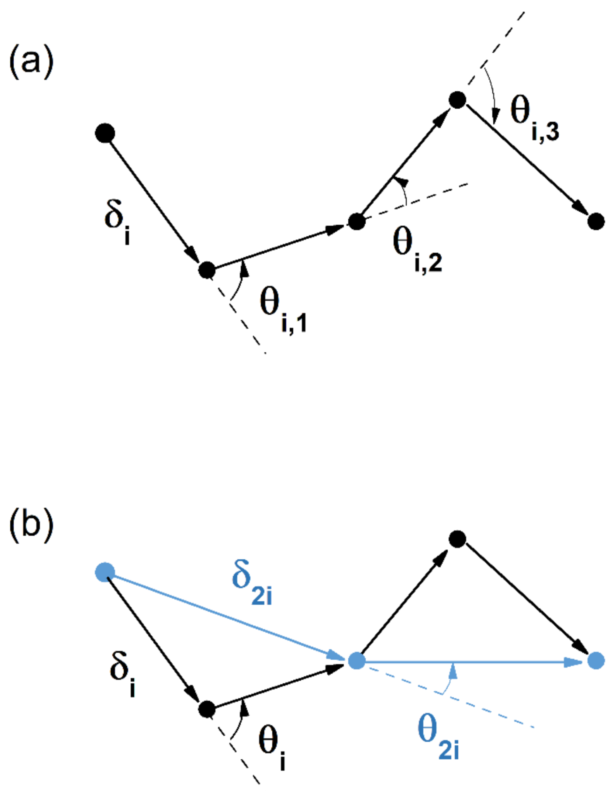

FIG. 3 (a) The random walker is seen at five locations (black dots) when the motion is observed with timescale τ_i, which gives rise to three successive turning angles $\theta_{i,1}$, $\theta_{i,2}$ and $\theta_{i,3}$. (b) When the timescale increases by two, that is τ_{2i}, the walker could only be seen at three locations (blue dots). Correspondingly one turning angle θ_{2i} is conceived. Vectors shown in black δ_i and blue δ_{2i} represent the net displacements of the walker during τ_i and τ_{2i}, respectively. The magnitude of δ_i is assumed to be constant.

We demonstrate the solution to Eq. (5) with $\theta_{2i} = 0$ as an example [and note that solving the equation with other θ_{2i} should yield the same result]. The first independent variable $\theta_{i,1}$ takes value freely within the complete range between $-\pi$ to π, however, it takes value from the complete range twice until all exclusive outcomes are exhausted. The second independent variable $\theta_{i,2}$ takes value in the range defined by $\theta_{i,1}$, specifically, $\theta_{i,2,\min} = -\frac{1}{2}\left(\theta_{i,1} + \pi\right)$ and $\theta_{i,2,\max} = -\frac{1}{2}\left(\theta_{i,1} - \pi\right)$ [Enumeration of $\theta_{i,1}$ and $\theta_{i,2}$ is detailed in Appendix B and C respectively]. Once both $\theta_{i,1}$ and $\theta_{i,2}$ are specified, there exists a unique $\theta_{i,3} = -\theta_{i,1} - 2\theta_{i,2}$ which satisfies the premise $\theta_{2i} = 0$. The Eq. (5) therefore yields to:

$$P(\theta_{2i} = 0, \rho_{2i}) = 2\int_{\theta_{i,1}=-\pi}^{\pi} \int_{\theta_{i,2}=-\frac{1}{2}(\theta_{i,1}+\pi)}^{-\frac{1}{2}(\theta_{i,1}-\pi)} P\left(\theta_{i,1}, \rho_i\right) P\left(\theta_{i,2}, \rho_i\right) P\left(-\left(\theta_{i,1} + 2\theta_{i,2}\right), \rho_i\right) \mathrm{d}\theta_{i,2} \mathrm{d}\theta_{i,1} \tag{6}$$

The right-hand side of Eq. (6) was solved using Monte-Carlo integration [27] and the resultant relationship between ρ_{2i} and ρ_i is plotted in Figure 4 as the solid line. The empirical datasets of $\rho_{2i}(\rho_i)$ determined from CRW simulation (shown as circles) agrees with the solution to Eq. (6). The dash-dot line in Figure 4 follows a hypothetical relationship $\rho_{2i} = \rho_i$ and it connects with the solution of Eq. (6) only at the two extremities: $\rho_{2i} = \rho_i = 1$ and $\rho_{2i} = \rho_i = 0$. These two connections imply that strict ballistic motion and fully-developed diffusion will remain so, independent of the changing timescale. On the other hand, when $0 < \rho_i < 1$, the solution to Eq. (6) always resides below the hypothetical $\rho_{2i} = \rho_i$ line. This dictates that ρ will always decrease with increasing τ, or in other words, the correlated random walk appearing ballistic will eventually manifest as diffusive upon prolonged observation. Our findings here agree with Bartumeus *et. al*'s work wherein they showed that the inflection in the random walker's $\langle \delta^2 \rangle$ scaling relationship [decrease in γ from 2 to 1] is inevitable, regardless of how close ρ_1 is to unity [11]. To conclude this part of discussion, we put forth the simpler expression in Eq. (7) which is obtained by performing a least square fit on the numerical solution to Eq. (6):

$$\frac{\rho_{2i}}{\rho_i} = \frac{1}{2}(\rho_i^2 + 1) \tag{7}$$

Note that the aforementioned deductions based on Eq.(6) is also captured by Eq. (7). Figure 5 (a), (b) and (c) shows the decrease in the effective value of ρ as a function of normalized timescale τ/τ_1 for random walkers starting with ρ_1 = 0.99, 0.95 and 0.50, respectively. The ρ values calculated using Eq. (6) and (7) are compared with that determined from CRW simulation.

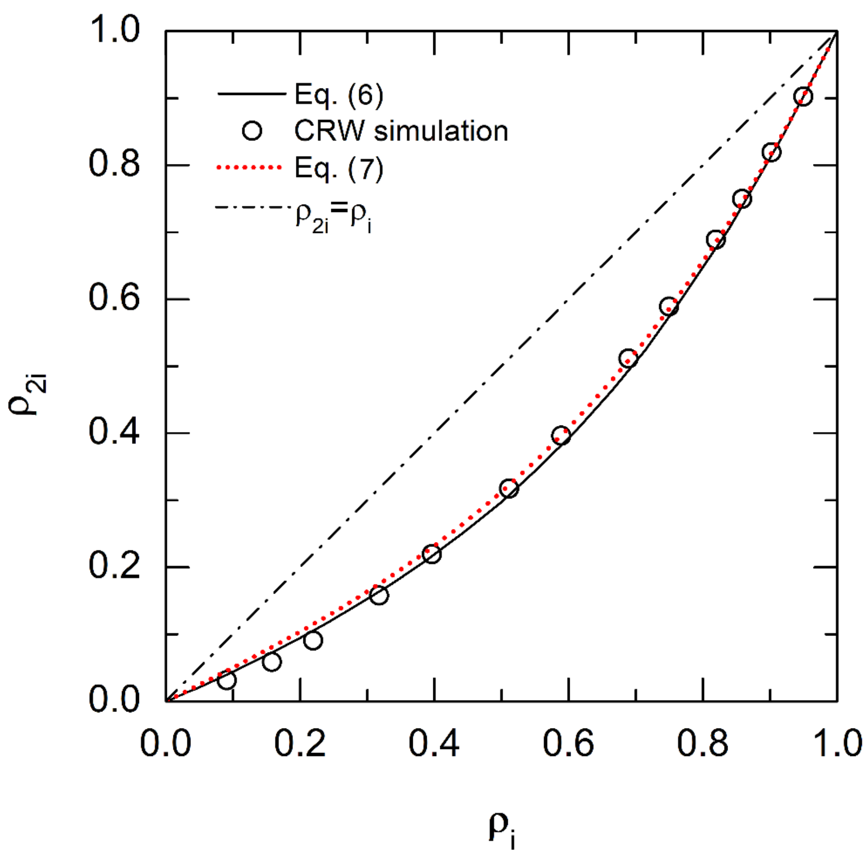

FIG 4. Relationship between ρ_{2i} and ρ_i. Solid line follows the solution to the analytical equation (6). Circles represent empirical datasets obtained from CRW simulation by performing least square fitting to the measured P(θ) at changing τ. Dotted line follow Eq. (7). The dash-dot line represents a hypothetical relationship $\rho_{2i} = \rho_i$.

We next connect the directional statistic interpretation of BD transition with the conventional spatio-temporal scaling relationship $\langle\delta^2\rangle \propto \tau^\gamma$ of the random walker. Per Figure 3(b) the walker's net displacement δ_{2i} during τ_{2i} could be related to the turning angle θ_i observed with τ_i [assuming constant net displacement δ_i during τ_i], that is $\delta_{2i}(\theta_i) = 2\delta_i\cos(\theta_i/2)$. Substitute the constant δ_i by $\langle\delta_i^2\rangle^{1/2}$ and the relationship yields to $\delta_{2i}(\theta_i) = 2\langle\delta_i^2\rangle^{1/2}\cos(\theta_i/2)$. Next, the ratio $\langle\delta_{2i}^2\rangle/\langle\delta_i^2\rangle$ equals to the trigonometric moment of the WCD function parameterized by ρ_i:

$$\langle\delta_{2i}^2\rangle/\langle\delta_i^2\rangle = 4\int_{-\pi}^{\pi}\cos^2(\theta_i/2)P(\theta_i,\rho_i)\,\mathrm{d}\theta_i \tag{8}$$

The exact analytical solution to Eq. (8) is:

$$\langle\delta_{2i}^2\rangle/\langle\delta_i^2\rangle = 2(\rho_i + 1) \tag{9}$$

Generalization of Eq. (9) yields the expression for the walker's normalized mean-square displacement $\langle\delta_{2^n}^2\rangle/\delta_1^2$ corresponding to timescale τ_{2^n}/τ_1 (where n is positive integer):

$$\langle\delta_{2^n}^2\rangle/\delta_1^2 = 2^n\prod_{m=1}^{n}(\rho_{2^{m-1}} + 1) \tag{10}$$

The solutions to equation sets (10) and (6) with ρ_1 = 0.99, 0.95 and 0.50 are plotted in Figure 5 (d)-(i) as the solid lines. Circles represent the empirical dataset obtained from the simulated random walk [$\langle\delta^2\rangle/\delta_1^2$ is calculated using Eq. (2) for simulation]. The comparison shows that our analytical solution gives accurate prediction to magnitude of the walkers $\langle\delta^2\rangle$ as well as the earliness of BD transition. Eq. (10) could be also solved along with the simple expression of Eq. (7), which gives reasonably accurate results (squares). Fig. 5 also shows that although the diffusive regime manifests earlier in the case of smaller ρ_1, the shape of the decreasing trends of γ and ρ appears invariant. This is because it always takes a fixed amount of time for ρ to decrease from one specific value to another per Eq. (6) [or (7)].

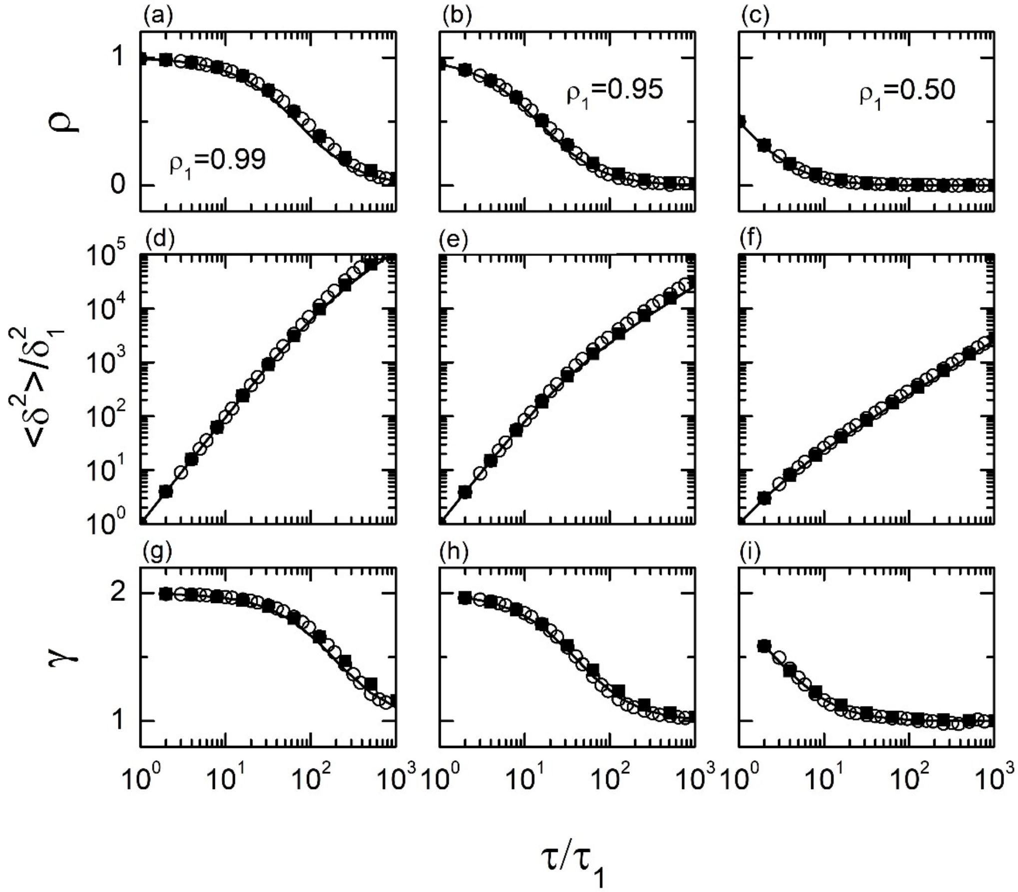

FIG 5. (a), (b) and (c) show the decrease in the effective value of ρ for random walker starting with ρ_1 = 0.99, 0.95 and 0.50, respectively. (d)-(f) show the corresponding normalized $\langle\delta^2\rangle/\delta_1^2 \sim (\tau/\tau_1)^\gamma$ scaling relationship. (g)-(i) show the evolution of the scaling exponent γ. In (a)-(c) solid lines represent solutions to equation Eq. (6). Circles represent empirical datasets obtained from CRW simulation. Squares follow Eq. (7). In (d)-(i) solid line represents solution to equation sets (6) and (10). Circles represent empirical datasets calculated from CRW simulation using Eq. (2). Squares represent solution to equation sets (7) and (10).

Rearranging Eq. (9) yields the relationship between $\gamma_{2\mathrm{i}}$ and ρ_{i}:

$$\gamma_{2\mathrm{i}} = 1 + \log_2(\rho_{\mathrm{i}} + 1) \tag{11}$$

which when solved with Eq. (6) or (7) provides the relationship between γ and ρ at a given τ. Figure 6 shows the relationship between γ and ρ obtained using our analytical formulations (solid and dotted lines) and from CRW simulation (circles). Good agreement is observed between the datasets.

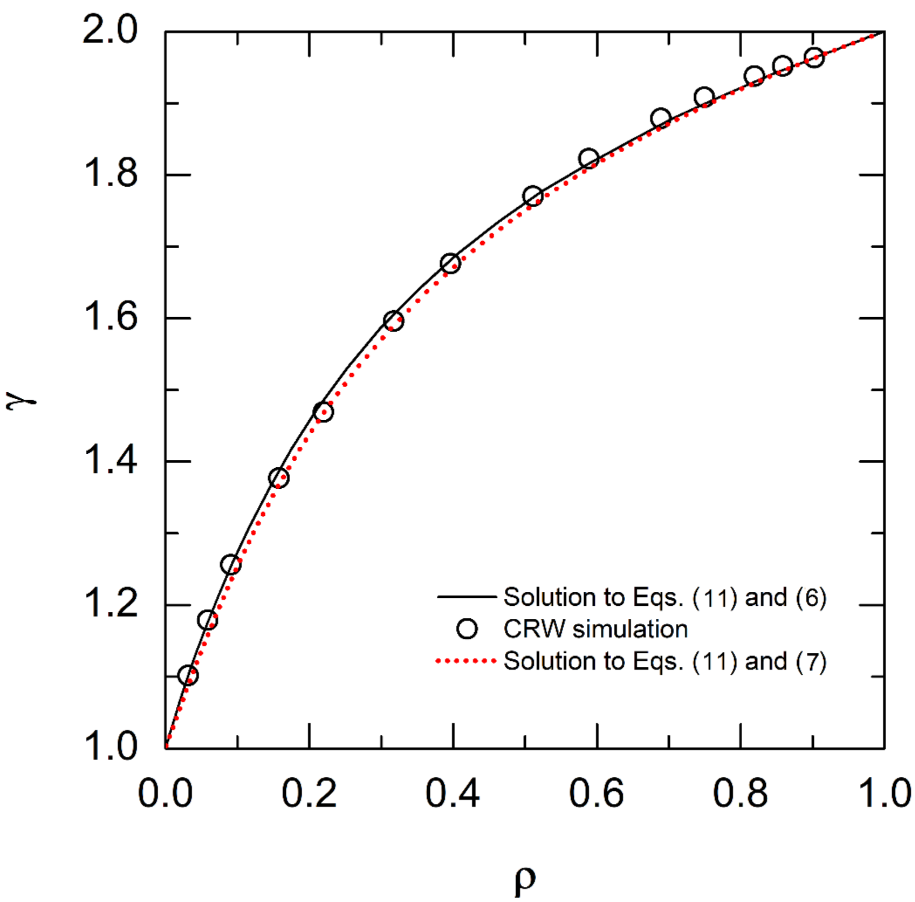

FIG 6. Relationship between γ and ρ. Solid line represents the solution to the equation set (11) and (6). Circles represent empirical datasets obtained from CRW simulation. Dotted line represents the solution to equation set (11) and (7).

V. CONCLUSION

We now bring together our major findings and conclude this work. Relationship between the two parameters ρ and τ is formulated using Eq. (6) [or (7)], and therefore the kinetics of BD transition is quantified. The one-to-one correspondence between ρ and γ is established using Eq. (11), such that our kinetic expression is tied to the conventionally used spatial-temporal scaling power-law. Figure 7 shows the contour plots for γ as a function of ρ_1 and τ/τ_1. Using this figure, one could roughly estimate the value of γ corresponding to a particular timescale. Use of the contour lines, however, is not recommended if an exact solution is desired. An accurate estimation of γ requires solving of the equation set (6) [or (7)] and (11). In addition, we emphasize that the robustness of WCD function in describing the walker's turning angle distribution remains to be tested experimentally for more complicated random walk processes, for example, particle motion in three-dimensional space with or without geometric confinements. The evolution of reorientation statistics for the random walk characterized with changing step-length distribution also requires further investigations [11]. We also point out that WCD is not the only function that finds applications in parametrizing random walk observed experimentally; future work will be directed toward generalizing the formulation presented in this work to the family of wrapped distribution functions [14-16].

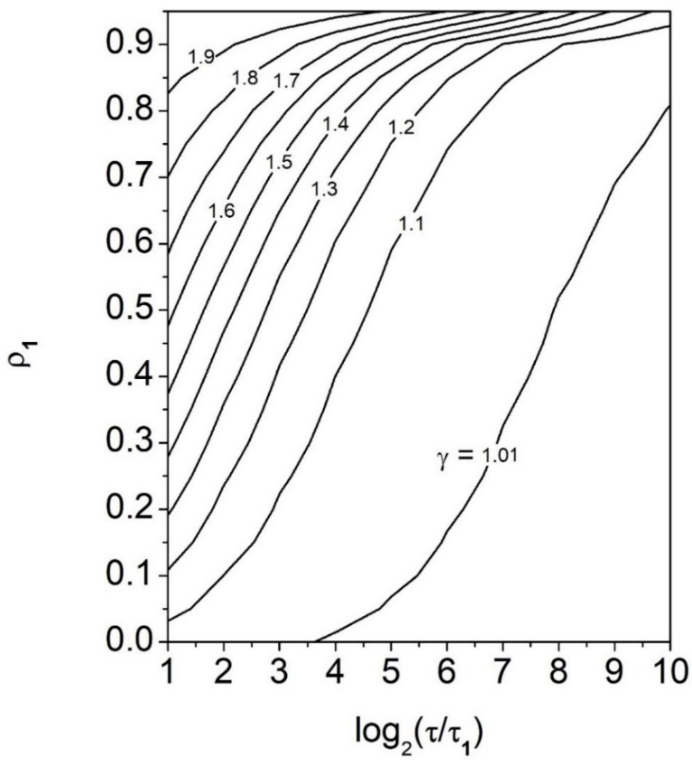

FIG 7. Contour plots of γ as a function of ρ_1 and normalized timescale τ/τ_1.

REFERENCE

[1] P. N. Pusey, Science **332,** 802-803 (2011).

[2] R. Huang *et al.*, Nat. Phys. **7,** 576-580 (2011).

[3] T. Li, S. Kheifets, D. Medellin, and M. G. Raizen Science **328,** 1673–1675 (2010).

[4] J. Blum *et al*., Phys. Rev. Lett**. 97,** 23060 (2006).

[5] J. Blum *et al*., Phys. Rev. Lett. **85,** 2426 (2000).

[6] W. D. Luedtke and U. Landman, Phys. Rev. Lett. **82,** 3835-3838 (1999).

[7] Y. Maruyama and J. Murakami, Phys. Rev. B **67,** 085406 (2003).

[8] T. H. Solomon, E. R. Weeks, and H. L. Swinney, Phys. Rev. Lett. **71**, 3975-3978 (1993).

[9] T. H. Solomon, E. R. Weeks, and H. L. Swinney, Physica D **76,** 70-84 (1994).

[10] H. P. Zhang, A. Be'Er, R. S. Smith, E. L. Florin, and H. L. Swinney, EPL **87,** 48011 (2009).

[11] F. Bartumeus, M. E. da Luz, G. M. Viswanathan, and J. Catalan, Ecology **86,** 3078-3087 (2005).

[12] W. M. Getz and D. Saltz, Proc. Natl. Acad. Sci. USA **105,** 19066-19071 (2008).

[13] R. N. Mantegna and H. E. Stanley, Phys. Rev. Lett. **73,** 2946-2949 (1994).

[14] K. V. Mardia and P. E. Jupp, *Directional Statistics* (John Wiley & Sons, New York, 2009).

[15] A. Lee, Wiley Interdiscip. Rev. Comput. Stat. **2,** 477–486 (2010).

[16] E. Batschelet, *Circular Statistics in Biology* (Academic Press, New York, 1981).

[17] J. H. Jeon *et al.*, Phys. Rev. Lett. **106,** 048103 (2011).

[18] J. H. Jeon *et al*., Phys. Rev. X **6,** 021006 (2016).

[19] F. Höfling and T. Franosch, Rep. Prog. Phys. **76,** 046602 (2013).

[20] C. Manzo and M. F. Garcia-Parajo, Rep. Prog. Phys. **78,** 124601 (2015).

[21] J. F. Reverey *et al*., Sci. Rep. **5,** 11690 (2015).

[22] J. W. Haefner, *Modeling Biological Systems: Principles and Applications* (Springer Science & Business Media, Berlin, 2005).

[23] R. Metzler, J. H. Jeon, A. G. Cherstvy, and E. Barkai, Phys. Chem. Chem. Phys**. 16,** 24128-24164 (2014).

[24] A. Andreanov and D. S. Grebenkov, J. Stat. Mech. P07001 (2012).

[25] S. Burov *et al*., Proc. Natl. Acad. Sci. USA **110,** 19689-19694 (2013).

[26] J. Masoliver, K. Lindenberg, and G. H. Weiss, Physica A **157,** 891-898 (1989).

[27] C. P. Robert *Monte Carlo Methods* (John Wiley & Sons, New York 2014).

ACKNOWLEDGEMENT

This work was supported by the US National Science Foundation (NSF) grants AGS-1455215 and CBET-1511964. We thank Prof. Richard L. Axelbaum, Prof. Christopher M. Sorensen and Kaifeng Xia for many constructive discussions.

APPENDIX A: DETERMINING θ FROM TRAJECTORY

The turning angle θ of could be determined from three successive positions of the walker, $[x(t), y(t)]$, $[x(t+\tau), y(t+\tau)]$ and $[x(t+2\tau), y(t+2\tau)]$, which are termed as A, B, and C, respectively. We calculate θ by finding the angle of $\overrightarrow{\mathrm{BC}}$ relative to $\overrightarrow{\mathrm{AB}}$. Note that θ takes value between $-\pi$ to π and counterclockwise is regarded positive for angle. Define φ_{AB} to be the angle of vector $\overrightarrow{\mathrm{AB}}$ relative to positive x-axis. Note that $\varphi_{\mathrm{AB}} \in [0, 2\pi)$, and it increases as $\overrightarrow{\mathrm{AB}}$ rotates around A along counterclockwise direction [$\varphi_{\mathrm{AB}} = 0$ when $\overrightarrow{\mathrm{AB}}$ is parallel to x and points to the positive direction]. We calculate the φ_{AB} as follows:

$$\varphi_{\mathrm{AB}} = k\pi + \arctan\left[\frac{y(t+\tau) - y(t)}{x(t+\tau) - x(t)}\right]$$

$$\text{and } \; k = \begin{cases} 0 & \text{if } x(t+\tau) > x(t) \text{ and } y(t+\tau) > y(t) \\ 1 & \text{if } x(t+\tau) < x(t) \\ 2 & \text{if } x(t+\tau) > x(t) \text{ and } y(t+\tau) < y(t) \end{cases} \tag{A1}$$

Similarly, we calculate the angle φ_{BC} of vector $\overrightarrow{\mathrm{BC}}$ relative to positive x-axis:

$$\varphi_{\mathrm{BC}} = k\pi + \arctan\left[\frac{y(t+2\tau) - y(t+\tau)}{x(t+2\tau) - x(t+\tau)}\right]$$

$$\text{and } \; k = \begin{cases} 0 & \text{if } x(t+2\tau) > x(t+\tau) \text{ and } y(t+2\tau) > y(t+\tau) \\ 1 & \text{if } x(t+2\tau) < x(t+\tau) \\ 2 & \text{if } x(t+2\tau) > x(t+\tau) \text{ and } y(t+2\tau) < y(t+\tau) \end{cases} \tag{A2}$$

At last, we calculate θ using φ_{AB} and φ_{BC}:

$$\theta = 2m\pi + \varphi_{\mathrm{BC}} - \varphi_{\mathrm{AB}}$$

$$\text{and } \; m = \begin{cases} 0 & \text{if } |\varphi_{\mathrm{BC}} - \varphi_{\mathrm{AB}}| < \pi \\ -1 & \text{if } |\varphi_{\mathrm{BC}} - \varphi_{\mathrm{AB}}| > \pi \text{ and } \varphi_{\mathrm{BC}} > \varphi_{\mathrm{AB}} \\ 1 & \text{if } |\varphi_{\mathrm{BC}} - \varphi_{\mathrm{AB}}| > \pi \text{ and } \varphi_{\mathrm{BC}} < \varphi_{\mathrm{AB}} \end{cases} \tag{A3}$$

APPENDIX B: ENUMERATION OF $\theta_{i,1}$

Define that a walker is seen at positions O, A, B, C and D when t increments by τ_i. Fig. 8 demonstrates the relationship between the turning angles and the corresponding vector pairs. Note that the following discussion is based on the assumption that the net displacement δ_i during τ_i is constant, or $|\overrightarrow{OA}| = |\overrightarrow{AB}| = |\overrightarrow{BC}| = |\overrightarrow{CD}| = \delta_i$. The counter-clockwise direction is regarded positive for angles.

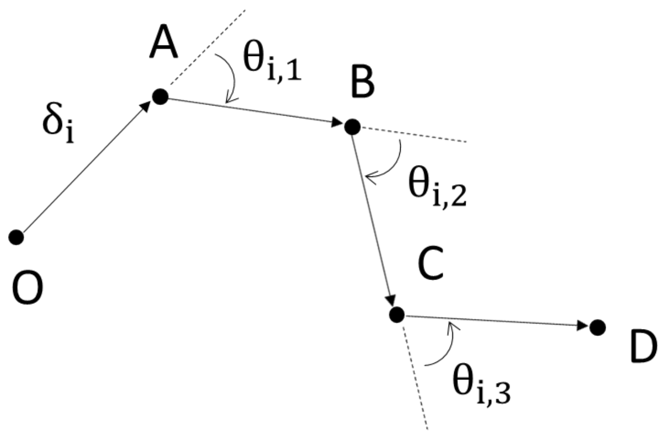

FIG. 8. When the walker is observed with timescale τ_i, it is seen at five successive locations O, A, B, C and D.

Next, set up a Cartesian coordinate with O serving as the origin and $\overrightarrow{OB}$ representing the positive x-axis [Fig. 9]. Define ω to be the angle of $\overrightarrow{OA}$ relative to positive y-axis. One could observe that the range for $\theta_{i,1}$ is unrestricted, and $\theta_{i,1}$ takes value from 0 to -2π twice before all possible configurations are exhausted. Specifically, an enumeration is outlined in the following:

(i). When ω decreases from 0 to $-\pi/2$, correspondingly A migrates from $(0, \delta_i)$ through the 1st quadrant to $(\delta_i, 0)$, $\theta_{i,1}$ increases from $-\pi$ to 0.

(ii) When ω decreases from $-\pi/2$ to $-\pi$, correspondingly A migrates from $(\delta_i, 0)$ through the 2nd quadrant to $(0, -\delta_i)$, $\theta_{i,1}$ increases from 0 to π.

(iii). When ω decreases from $-\pi$ to $-3\pi/2$, correspondingly A migrates from $(0, -\delta_{\rm i})$ through the 3rd quadrant to $(-\delta_{\rm i}, 0)$, $\theta_{i,1}$ increases from $-\pi$ to 0.

(iv). When ω decreases from $-3\pi/2$ to -2π, correspondingly A migrates from $(-\delta_{\rm i}, 0)$ through the 4th quadrant to $(0, \delta_{\rm i})$, $\theta_{i,1}$ increases from 0 to π.

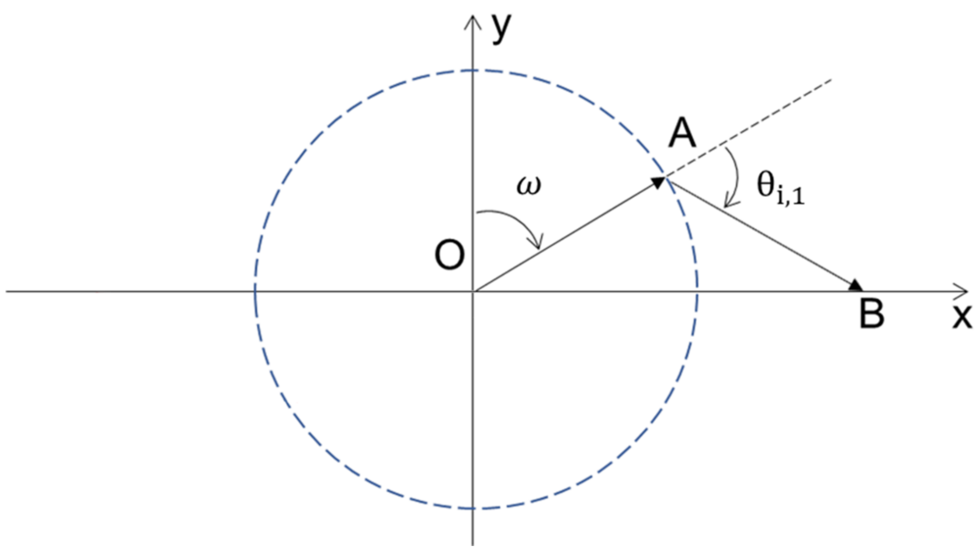

FIG. 9. Enumeration of $\theta_{i,1}$.

APPENDIX C: ENUMERATION OF $\theta_{i,2}$

The range for $\theta_{i,2}$ is discussed under the condition that both $\theta_{i,1}$ and θ_{2i} are specified. Note that $\theta_{i,1}$ could take any arbitrary value but $\theta_{2i} = 0$. Per Fig. 10 segment PQ which is perpendicular to x-axis passes it through B. The half-circle [dashed curve] has a radius of δ_i and it intercepts with the x-axis at R. Note that since vector $\overrightarrow{OB}$ is set as positive x, the condition $\theta_{2i} = 0$ requires that $\overrightarrow{BD}$ also resides on x-axis and points to the positive direction. In other words, vector $\overrightarrow{CD}$ has to connect with x-axis at the position D satisfying $x_D > x_B$.

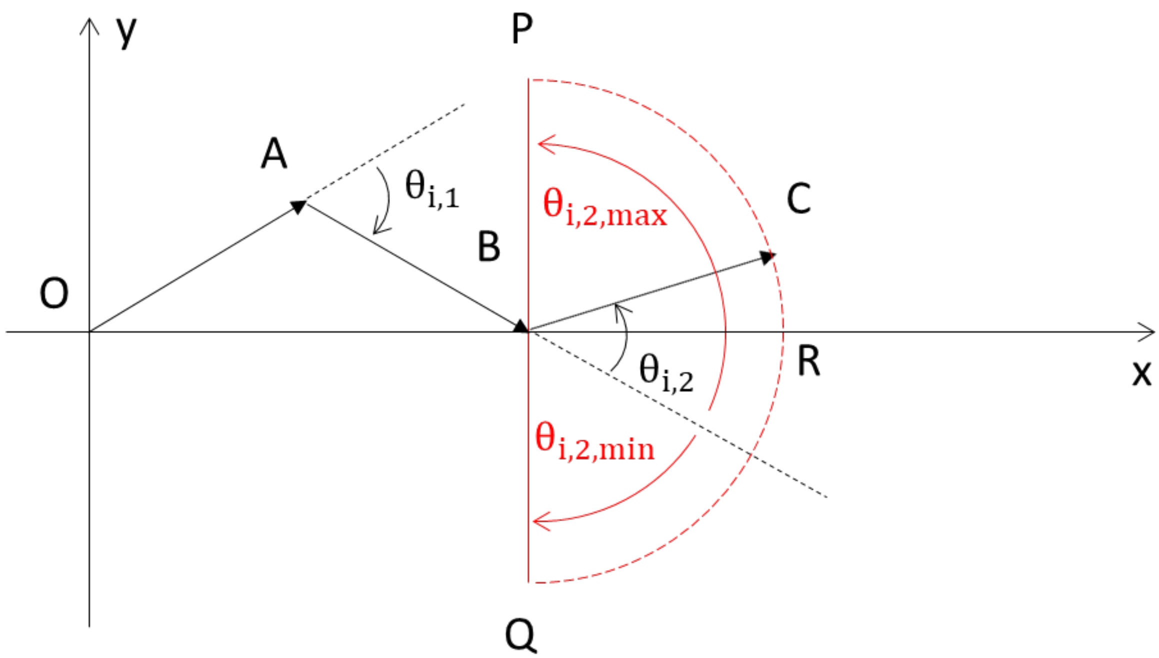

FIG. 10. Enumeration of $\theta_{i,2}$.

The half circle $\widehat{PRQ}$ exhausts all possible positions for C under the premise of $\theta_{2i} = 0$. In other words, C could only reside on $\widehat{PRQ}$ such that the vector $\overrightarrow{CD}$ could subsequently connect x-axis at D with a constant length δ_i. The maximum and minimum of $\theta_{i,2}$ [indicated in Fig. 10 by the red arrows] are dictated by the value of $\theta_{i,1}$, which could be written as: $\theta_{i,2,\min} = -\frac{1}{2}(\theta_{i,1} + \pi)$ and $\theta_{i,2,\max} = -\frac{1}{2}(\theta_{i,1} - \pi)$.